# Risk Assessment of Coupled Hazardous Scenarios

Chen, Chao; Reniers, Genserik; Yang, Ming

**Important note**
To cite this publication, please use the final published version (if applicable).
Please check the document version above.

# Chapter 4
# Risk Assessment of Coupled Hazardous Scenarios

## 4.1 Introduction

In the process and chemical industry,[1] major accident scenarios such as fire, explosion, and toxic gas dispersion may occur due to the loss of containment of hazardous materials [3–6]. Among these major accident scenarios, fire is the most common scenario (44%), followed by explosion (36%). 20% of all major accidents are only toxic dispersion without fire and explosion, while 30% of the explosion and fire scenarios involve toxic substances [7]. Since chemical industrial areas are usually congested with many hazardous installations, a fire or explosion may lead to domino effects, resulting in multiple accident scenarios. As a result, major accident scenarios such as fire, explosion, and toxic release can simultaneously or sequentially be present in one disaster due to the evolution of domino effects.

In light of past disasters listed in Chap. 3 and since unpredicted hazards may result in severe consequences, modeling the spatial–temporal evolution of hazards and events originating from a release of hazardous materials in industrial areas is essential for protecting staff, residents, and emergency rescuers. For example, in the Tianjin port disaster in 2015, caused by the spontaneous ignition of nitrocellulose, many of the emergency rescuers were killed in the disaster due to an unpredicted evolution of the fire to an explosion. To avoid such catastrophic disasters, many post-accident analyses were conducted on the prediction of overpressure induced by explosions [8–12] and vapor cloud dispersion [13–15]. Besides, a lot of work has been done on vulnerability assessment of installations to VCEs, risk assessment of domino effects caused by VCE [16–21] and domino effects triggered by fire [22–24]. In terms of the evolution of fire, the time to failure of equipment subject to fire is critical for the vulnerability of installations [25]. As a result, dynamic methods were used to assess the vulnerability of installations exposed to fire and fire-induced domino effects [26–29]. Among these dynamic tools, both the dynamic graph approach and

---

[1] This chapter is mainly based on two publications: Chen et al. [1] and Chen [2].

95

the dynamic Bayesian network approach can model the spatial–temporal evolution of domino effects caused by fire and visualize the escalation paths of fire [3, 26]. Besides, Monte Carlo simulation was used to address the evolution uncertainty of domino effects [30–32].

In view of the research attempts on VCE hazard or fire hazard evolution, little attention has been paid to dynamic hazard evolution of possible toxic release, VCE and fire in a catastrophic disaster, and the assessment of human exposure to multiple hazards sequentially. This chapter, therefore, aims to establish a dynamic method for human and facility vulnerability assessment considering the spatial–temporal evolution of multiple hazards such as toxic release, VCE, and fire. Both the uncertainty of ignition and the uncertainty of the evolution of different hazards are considered in the present study. The dynamic graph model is developed in Sect. 4.2. The graph update rules and a simulation algorithm based on dynamic Monte Carlo simulation are introduced in Sect. 4.3. The conclusions drawn from this chapter are summarized in Sect. 4.4.

## 4.2 Modeling

Agent-based modeling (ABM) is a powerful modeling technique that has been widely used in many domains in recent decades, such as complex adaptive systems, biology, business [33]. Compared with other modeling tools based on events or processes, ABM focuses on agent behaviors (attributes and interactions), and it is very flexible to model socio-technical systems [30, 34, 35]. Graph-based methods can provide a visible structure (graph or network) to represent the complex agent interactions. Consequently, graph-based approaches are often used to model interacting agents in a system [36, 37]. By applying graphs, the agents are represented by nodes, and their dependencies are denoted by edges [23, 38, 39]. According to this principle, a chemical plant can be regarded as a system (a graph), while the hazardous installations within the plant can be modeled as agents (nodes). In that case, graph metrics such as in-closeness and out-closeness can be used to assess the domino effect potential and the damage likelihood of installations being damaged by escalation effects [23, 40]. The spatial–temporal evolution characteristics of fire-induced escalations can then be addressed by dynamic graphs [27].

In terms of modeling the evolution between different accident scenarios, it is difficult to address the uncertainty in scenario evolution by merely using the dynamic graph approach. To deal with the uncertainty, the Monte Carlo method can be integrated with the dynamic graph approach. Monte Carlo simulation is a commonly used tool to model uncertainties and avoid complex mathematical calculations [41–43]. The new integrated approach based on dynamic graphs and Monte Carlo simulation is called Dynamic Graph Monte Carlo (DGMC). The DGMC is an ABM method consisting of a dynamic graph with random parameters and a Monte Carlo simulation for modeling uncertainties.

According to the developed DGMC method, we can model the evolution of multiple accident scenarios in coupled domino effect events and dynamically assess human vulnerability exposed to these scenarios. The DGMC is defined as a dynamic graph with a nine-tuple, as follows:

$$DGMC = (M, N, K, C, O, Q, T) \qquad (4.1)$$

### 4.2.1 Graph Nodes

In the DGMC model, graph nodes are used to model installations ($N$), human positions ($M$), and ignition sources ($K$).

(1) **Hazardous installations**

$n$ represents the numbering of hazardous installations, and a total of $N$ installations are assumed in a chemical plant. According to possible major accidents in industrial areas and the vulnerability characteristics of hazardous installations, the states of hazardous installations are divided into five types, as shown in Table 4.1.

The state "operational" is an initial state indicating that the installation is undamaged and operational. The state "extinguished" is a termination state in which the installation is damaged without any hazardous effects. Unstable states of "release", "fire" and "VCE" represent major accident scenarios of the loss of containment of hazardous materials, fire, and vapor cloud explosion, respectively. These unstable states can be harmful to installations and humans. The state of "fire" is caused by an immediate ignition, while the state of "VCE" results from delayed ignition. Table 4.2 shows human states, including one initial state "safe" and two terminal states "injured" and "dead".

**Table 4.1** States of hazardous installations (Chen et al. [1])

| State | Description |
| --- | --- |
| Operational | The hazardous installation is not physically damaged and is operational |
| Release | The hazardous installation is physically damaged, resulting in the loss of containment of hazardous materials and/or poisoning humans nearby |
| Fire | The installation is on fire due to immediate ignition, causing heat radiation on humans and/or other installations |
| VCE | The installation's loss of containment induces a vapor cloud explosion due to delayed ignition |
| Extinguished | The installation is physically damaged but does not generate any hazardous effects |

**Table 4.2**  Human states (Chen et al. [1])

| State | Description |
|---|---|
| Safe | The human does not receive any hazardous effects |
| Injured | The human is injured due to exposure to toxic gas, heat radiation, or overpressure |
| Dead | The human is decreased due to exposure to toxic gas, heat radiation, or overpressure |

**Table 4.3**  States of ignition sources (Chen et al. [1])

| State | Description |
|---|---|
| Inactive | Flammable vapor is not present at the ignition source, or the vapor concentration is out of the flammability limit |
| Active | Flammable materials are present at the ignition source, and the concentration of the vapor is between the lower and upper flammability limits |
| Ignited | The ignition source has ignited the flammable vapor |

(2)  **Human positions**

$m$ represents the numbering of human positions in which humans may suffer from toxicity from toxic gases, heat radiation caused by fire, or overpressure induced by VCEs. A total of $M$ human positions are assumed in the chemical plants. People at different places and times may suffer different hazardous effects caused by major accident scenarios. According to possible hazardous effects and human vulnerability characteristics in a chemical plant, the states of humans are divided into three types, as shown in Table 4.2.

According to Table 4.2, a person in a chemical plant may either (i) be safe without any hazardous effects or (ii) may be injured or (iii) may be dead due to hazardous effects.

(3)  **Ignition sources**

$k$ represents the numbering of ignition sources that may ignite flammable gases. According to ignition requirements, the states of ignition sources can be categorized into three types: "inactive", "active" and "ignited", as shown in Table 4.3.

As shown in Table 4.3, the states of ignition include one initial state (inactive), one terminal state (ignited), and one intermediate state (active). It should be noted that all the preceding states are time-dependent and may be updated with the spatial–temporal evolution of the hazards.

### 4.2.2  Graph Edges

In the DGMC model, directed edges represent the hazardous effects that may cause damage to hazardous installations or be harmful to humans. In this chapter, we

consider three types of hazardous effects: the heat radiation induced by fire, the overpressure caused by VCEs, and the toxicity induced by a toxic cloud. Accordingly, we defined four types of directed edges: the ignition effects from released installations to ignition sources, the toxic effects from installation nodes to human nodes, the heat radiation from installation nodes to installation nodes or human nodes, and the overpressure effects from installation nodes to installation nodes or human nodes.

(1) **Delayed ignition**

If the hazardous materials which have been released are ignited immediately, no directed edges need to be established between release installations and ignition sources. Otherwise, when a flammable gas covers an ignition source, a directed edge from the installation where the material was released towards the ignition source should be established. If the flammable gas is ignited subsequently, all the directed edges from the released installations where materials have been released to ignition sources should be removed.

(2) **Acute intoxication**

If a human position is covered by toxic gas, a directed edge should link the released installation where the toxic material was released and the person's position. The acute intoxication of humans at the position covered by a toxic gas is determined by the toxic concentration ($C_t$) and exposure time ($t_e$). In this chapter, the probit function of acute intoxication [44] is used to obtain the death probability caused by human exposure to toxic gas, as follows:

$$Y_t = c_7 + c_8 \ln\left(C_t^{c_9} \times t_e\right) \tag{4.2}$$

$Y_t$ represents the probit value of human vulnerability exposure to toxic gas. $c_7$, $c_8$, and $c_9$ represent the parameters of the probit function that change with different toxic substances. These parameters for some common toxic materials can be obtained from Van Den Bosh et al. [44]. Besides the toxic concentration and exposure time, other factors such as demographics (e.g., ages) and Personal Protection Equipment (PPE) may partially affect the death induced by toxic gases. For instance, if an employee wears a gas mask, the likelihood of death caused by toxic gas can be significantly reduced due to the filtering effect induced by the mask.

(3) **Damage induced by VCEs**

Since overpressure can damage installations and be harmful to humans, directed edges should be established from the installation where the overpressure generates to both installations and human positons. In the DGMC model, $O$ represents the directed edge caused by overpressure. As illustrated in Chap. 3, several methods for overpressure calculation are available, such as the TNT equivalent method, the Baker-Strehlow method, and CFD simulation. The TNT equivalent method is a simple method based on the TNT explosion mechanism, neglecting the effects of space configuration, ignition sources, and flammable gas distribution. As a result, applying

**Table 4.4**  Probit function parameters of overpressure (Chen et al. [1])

| Installations | Atmospheric | Pressurized | Elongated | Auxiliary | Human |
|---|---|---|---|---|---|
| $c_5$ | −9.36 | −14.44 | −12.22 | −12.42 | −77.1 |
| $c_6$ | 1.43 | 1.82 | 1.65 | 1.64 | 6.91 |

the TNT equivalent method in VCE estimation may underestimate the overpressure. The Multi-Energy method is developed for gas explosions by dividing an explosion into a number of sub-explosions and considering the roles of congestion levels, ignition, and gas distribution in obstructed areas. For quantitative analysis, the Netherlands Organization for Applied Scientific Research (TNO) recommends the Multi-Energy method [45]. Therefore, the Multi-Energy method [46] is adopted in this chapter for calculating the overpressure intensity received by different installations and humans. More details related to this method are described in Chap. 3.

The damage probability of hazardous installations and the death probability induced by overpressure can also be calculated by applying probit functions. The damage probability of installations and the death probability of humans depend on the overpressure intensity and the vulnerability characteristics of installations and humans exposed to overpressure, as follows:

$$Y_p = c_5 + c_6 \ln(P_o) \tag{4.3}$$

$Y_p$ denotes the probit value with respect to overpressure generated by VCEs. $c_5$ and $c_6$ represent parameters related to the vulnerability characteristics of installations and humans, as shown in Table 4.4.

(4)  **Damage induced by fires**

The heat radiation induced by fire can be harmful to humans and installations. If an installation is on fire, directed edges should be added from the installation to other installations and humans. $Q$ is a matrix representing the heat radiations generated by installations in "fire" states. $q_{i,j}$ is an element of the matrix representing the heat radiation induced by an installation $i$ in a "fire" state to an installation or a human $j$, as follows:

$$Q = \begin{bmatrix} 0 & q_{1,2} & \cdots & q_{1,m+n} \\ q_{2,1} & 0 & \cdots & q_{2,m+n} \\ \cdots & q_{i,j} & 0 & \cdots \\ q_{m,1} & \cdots & q_{m,m+n-1} & q_{m,m+n} \end{bmatrix} \tag{4.4}$$

$q_{i,j}$ can be calculated by the application of ALOHA. It should be remarked that $Q$ is not a square matrix in this chapter since humans can only receive but not induce heat radiation. Considering possible synergistic effects [3] caused by multiple installations in the "fire" states, the heat radiation received by an installation or human $j$ ($Q_j$) can be obtained, as follows:

$$Q_j = \sum_{i=1}^{m} q_{i,j} \tag{4.5}$$

According to the heat radiation matrix, the Domino Evolution Graph (DEG) model developed in Chap. 2 can be applied to calculate the evolution caused by heat radiation and thus obtain the heat radiation received by humans at different evolution times. Then the death probability of humans exposed to heat radiation can be calculated by using the exposure time and the received heat radiation ($Q$), as follows:

$$Y_f = -14.9 + 2.56 \ln\left(6 \times 10^{-3} \times Q^{1.33} \times t_e\right) \tag{4.6}$$

$Y_f$ denotes the probit value with respect to the heat radiation generated by fire. However, the heat radiation received by humans ($Q$) may vary with the evolution of domino effects since the number of hazardous installations in the "fire" state may change during the evolution. Therefore, the hazardous effects caused by heat radiation at different periods should be superimposed to determine human vulnerability. As a result, at the evolution time $T_g$, the probit value ($Y_{f,T_g}$) can be obtained, as follows:

$$Y_{f,\,t_G} = -14.9 + 2.56 \ln\left(6 \times 10^{-3} \times \sum_{g=1}^{g=G} \left(Q_g^{1.33} \times t_g\right)\right) \tag{4.7}$$

The number of people at risk (exposed to accidental scenarios) can also change with the expansion of the accidental area due to domino effects.

### 4.2.3   Evolution Time

$T$ represents the evolution time of a domino effect event. $T$ is equal to zero when a loss of containment of hazardous materials emerges. The DGMC is divided into $G$ static graphs ($G$ nodes) due to the evolution of domino effects. The parameters of DGMC are updated at each time node $T_g$ due to the change of ignition states, human states, and installation states. In the initial stage, the evolution time mainly depends on the ignition time ($IT$). $IT$ is an uncertain variable determined by the number of ignition sources, ignition effectiveness, and vapor cloud dispersion, etc. The $IT$ is equal to zero if the released materials are immediately ignited, while it equals the delayed time when it is a delayed ignition. If there is no ignition, the $IT$ is infinite. The likelihood of immediate ignition mainly depends on the autoignition of flammable substances and the static discharge caused by the release [47]. If the ignition is delayed, the likelihood of ignition caused by a single ignition source is determined by the ignition effectiveness and the period that the ignition source is covered by

the flammable vapor. If there are multiple ignition sources at different positions, the possible ignitions caused by various ignition sources can be considered to be independent events. Thus, the total ignition probability caused by multiple ignition sources can be obtained, as shown in Chap. 3.

## 4.3   Graph Update Rules and Simulation Algorithm

### 4.3.1   Graph Update Rules

According to the DGMC model, the graph update rules should be determined to develop the simulation algorithm. The possible state transitions and physical effects in the DGMC model are illustrated in Fig. 4.1.

The dotted lines denote the state transition of nodes (e.g., installations, ignition sources, and humans), while solid lines represent the hazardous effects caused by a node to other nodes. Due to any intentional or unintentional causes, a loss of containment of hazardous materials from an installation may occur, resulting in the state of the installation changes from "operational" to "release". The installation in the "release" state can transfer to a "fire" state if the released materials are ignited immediately. But it may transfer to a "VCE" state if the ignition is delayed. Besides,
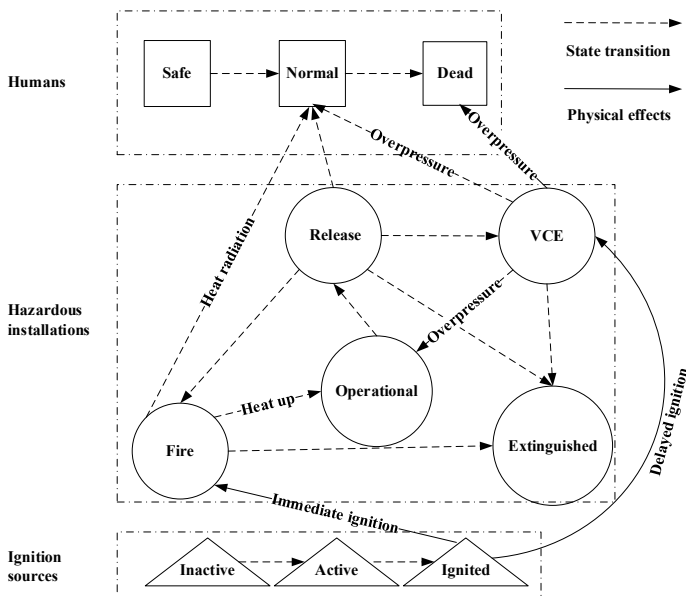


**Fig. 4.1**   State transition and hazardous effects (Chen et al. [1])

Humans may be injured due to the exposure to toxic gases released from installations, heat radiation generated by installations on fire, and overpressure induced by VCEs caused by a delayed ignition. Moreover, people may die due to prolonged exposure to heat radiation or toxic gases, while they may immediately die due to overpressure because the death likelihood caused by explosions is only determined by the overpressure intensity without the exposure time. In a coupled domino effect, humans may suffer from different accident scenarios at different evolution times and different positions.

To further illustrate the graph update rules, a simple example of a DGMC model with nine static graphs is given in Fig. 4.2. As shown in Fig. 4.2a, the state of the hazardous installation T1 changes from "operational" to "toxic release" when a toxic material releases from an installation. If the released material is ignited immediately, the installation's state will change to "fire" and induce heat radiation on humans and other installations. Otherwise, a flammable vapor cloud may form and disperse along with the vaporization of the release material, resulting in acute toxicity of humans (as shown in Fig. 4.2b). With the dispersion of vapor cloud, the ignition source S1 is covered by the flammable gas, and its state changes from an "inactive" state to an "active" state, as shown in Fig. 4.2c. A VCE occurs when the vapor cloud is ignited by S1, resulting in the damage of hazardous installations and casualties. As shown in Fig. 4.2d, a loss of containment scenario occurs at T2 and T4 while T3 is not damaged by the overpressure. Besides, Humans at H1 and H2 are exposed to the overpressure caused by the VCE. They are injured, but H1 may be more severe than that of H2 due to the synergistic effect caused by the exposures to the toxic gas and the overpressure at H1. Simultaneously, T2 and T4 are on fire due to an immediate ignition, as shown in Fig. 4.2e. In other words, the possible time delay between the explosion (Fig. 4.2d) and fire (Fig. 4.2e) is not considered in this study. In terms of the subsequent scenarios of VCE, they are more likely to be on fire since the explosion can release a lot of heat and energy, increasing the likelihood of immediate ignition at the two damaged tanks. Next, synergistic effects are induced by the two tanks in "fire" states on tanks H1, H2, and T3. As shown in Fig. 4.2f, humans at H1 die at time $t_5$ due to the accumulation of exposure to heat radiation. Similarly, H2 dies at evolution time $t_6$, as shown in Fig. 4.2g. At $t_7$ (Fig. 4.2h), the state of T4 transfers from "fire" to "extinguished" due to the burn-out of flammable substances or firefighting actions. Finally, the fire at T2 is also extinguished, and thus T3 survives since no escalation vectors exist, as shown in Fig. 4.2i.

### 4.3.2  Simulation Algorithm

The dynamic evolution of a coupled domino effect is represented by a dynamic graph (see Fig. 4.2). Due to the evolution of uncertainties such as the ignition time and the accident scenarios in coupled domino effects, numerous dynamic graphs should list all the possible evolution paths. Besides, more dynamic graphs are needed for real chemical industrial areas with multiple ignition sources and a vast variety of
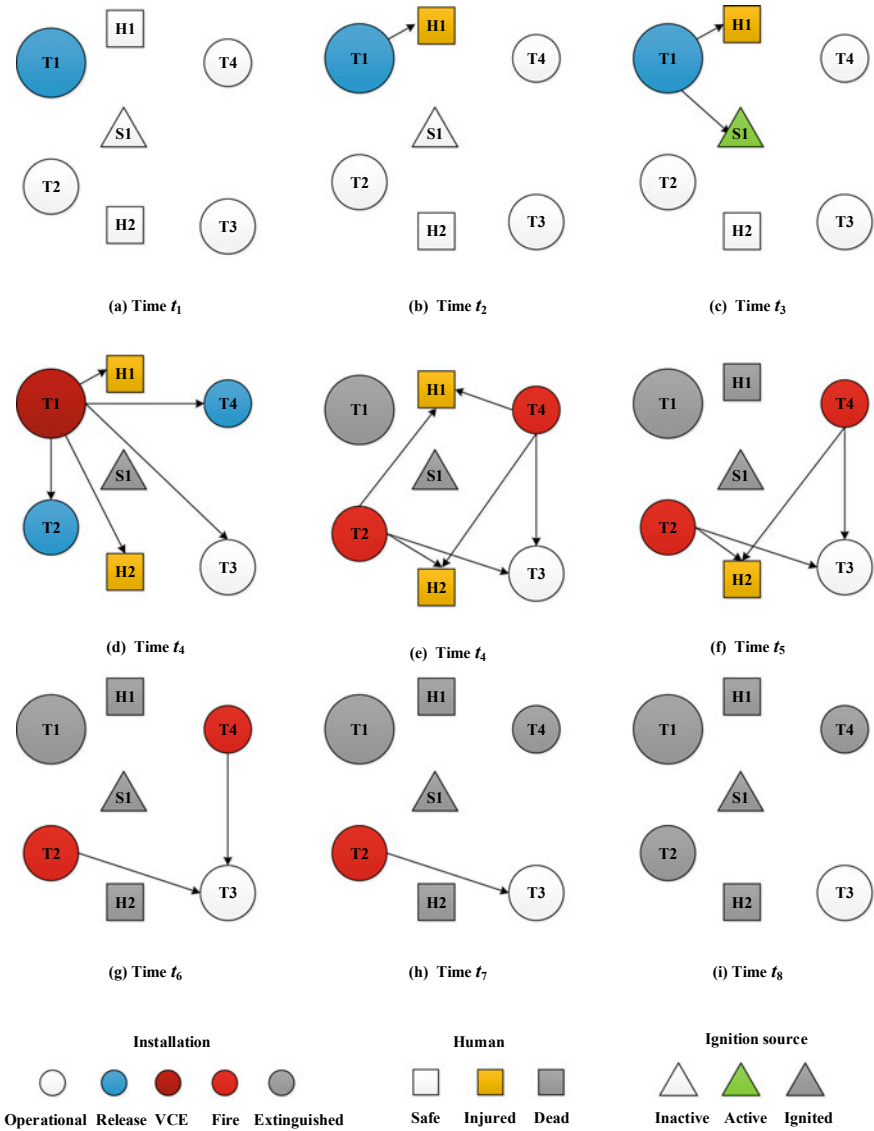
(a) Time $t_1$

(b) Time $t_2$

(c) Time $t_3$

(d) Time $t_4$

(e) Time $t_4$

(f) Time $t_5$

(g) Time $t_6$

(h) Time $t_7$

(i) Time $t_8$

| Installation | | | | | Human | | | Ignition source | | |
|---|---|---|---|---|---|---|---|---|---|---|
| Operational | Release | VCE | Fire | Extinguished | Safe | Injured | Dead | Inactive | Active | Ignited |

**Fig. 4.2**  A DGMC with nine static graphs (Chen et al. [1])

hazardous installations. To be able to cope with this situation, an algorithm based on Monte Carlo simulation is developed to generate dynamic graphs, tackling the time-dependencies and uncertainties in coupled domino effects. Figure 4.3 shows the developed algorithm based on the Monte Carlo simulation for solving the DGMC model.
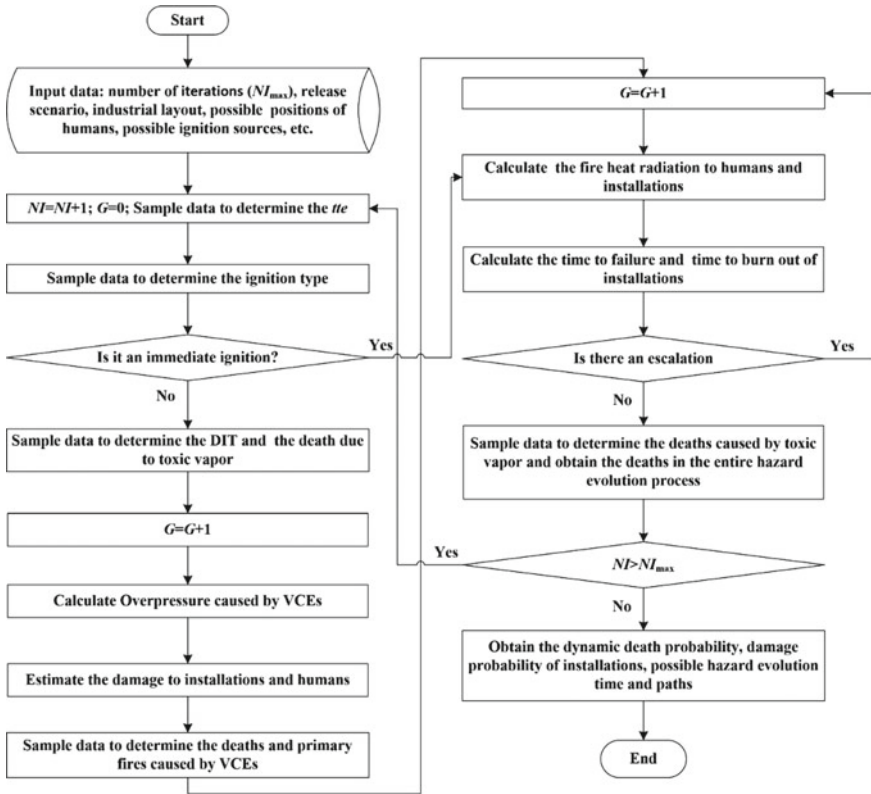
**Fig. 4.3** Simulation algorithm based on Monte Carlo method (Chen et al. [1])

As shown in Fig. 4.3, the first step of the algorithm is to input all the needed basic data related to the chemical plant, such as the number of iterations ($NI_{max}$), the industrial layout, release scenarios, possible ignition sources, etc. Step 2 determines the ignition type using random sampling. If it is a delayed ignition, the ignition time ($IT$) and the ignition source are determined by random sampling; otherwise, the ignition time equals zero. Then the death caused by the exposure to toxic gases can also be determined using Eq. (4.2). At the $IT$, the dynamic graph should be updated, and the edges in the graph represent overpressure induced by the VCE. The death probability caused by overpressure for humans and hazardous installations can be calculated according to Eq. (4.3). The fatalities and damaged installations are determined by using random sampling. The graph will be updated again when a fire occurs, and the edges in the graph represent heat radiations from the installation on fire to other installations. Next, the time to failure of hazardous installations can be determined using the method illustrated in Chap. 2. If there is an immediate ignition, the calculation procedures for explosion and toxic vapor can be overlooked, and only the calculation related to fire escalation is conducted. During the fire escalation

period, the graph is updated when a new fire occurs or an existing fire is extinguished when the evolution is over.

The above calculation steps will be repeated $NI_{max}$ times. Finally, the death probability of humans and failure probability of installations during the dynamic evolution of coupled domino effects are obtained. Besides, we can also obtain the possible evolution paths, evolution time nodes, and ignition times by using the algorithm.

## 4.4   Case Study

To illustrate the approach, a chemical storage facility with 37 chemical storage tanks (T1–T37), 5 possible human positions (H1–H5), and two possible ignition sources (S1–S2) is used as a case study. Table 4.5 lists the main features of storage tanks. The layout of the storage plant is shown in Fig. 4.4.

An overfilling of acrylonitrile at T1 with a filling rate of 100 kg/s is considered the primary scenario. The release of acrylonitrile can result in acute intoxication and

**Table 4.5**  Features of storage tanks (Chen et al. [1])

| Tank | Dimension × Height (m) | Chemical substance | Nominal volume (m$^3$) | Chemical content (m$^3$) |
| --- | --- | --- | --- | --- |
| T1–T6 | 21.0 × 16.6 | Acrylonitrile | 5000 | 4000 |
| T7–T9, T12–T15 | 17.0 × 15.4 | Gasoline | 3000 | 2400 |
| T10, T11 | 7.0 × 13.6 | Gasoline | 500 | 400 |
| T16–T27 | 14.5 × 12.7 | Gasoline | 2000 | 1600 |



**Fig. 4.4**  Chemical storage facility considered in the case study (Chen et al. [1])
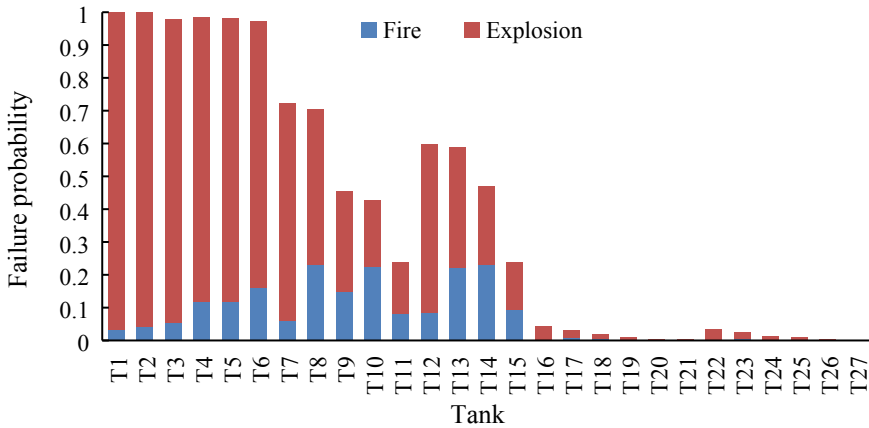
**Fig. 4.5** Failure probabilities of tanks caused by fire and explosion (Chen et al. [1])

possible subsequent explosions and fires may lead to overpressure and heat radiation. The ambient temperature is 0 °C and the wind speed is equal to zero. According to the vapor cloud dispersion model, the ignition source S1 is in the "active" state after 5.1 min and S2 is in the "active" state after 2.8 min. The autoignition probability $P_{ia}$ is zero and the ignition probability due to static discharge $P_{is}$ is 0.02, the autoignition temperature is 481 °C [48]. The possible heat radiations induced by tanks and the burning rates of fires are calculated through the ALOHA software. The number of iterations ($NI_{max}$) is set as $10^5$ and the computation time is 3.9 min.

Figure 4.5 shows the failure probabilities caused by possible fires and explosions due to the overfilling of acrylonitrile at T1. The failure probabilities of T1-T6 are near 1 since they are close to the release tank. The failure probabilities of tanks obviously decrease with increasing the distance between the release sources and the tanks (e.g., T7–T11, T12–T15). Based on the probabilities caused by fire and explosion of each tank, the tanks close to T1 (i.e., T1–T8 and T12) are more likely to be directly damaged by VCEs. These damaged tanks may catch fires and escalate spatially as well as temporally, resulting in the damage of other tanks such as T10 and T11.

Due to the spatial–temporal evolution of accident scenarios, people may suffer from different hazardous accident scenarios. The death probabilities caused by different scenarios at H1–H5 are shown in Fig. 4.6. The total death probabilities at H1 and H2 are around 0.99, indicating that people at H1 and H2 are very likely to die due to exposure to toxic gas or fire. The death probability caused by fire and toxic gas at H1 and H2 are approximately identical, which indicates that people at H1 and H2 may simultaneously or sequentially receive the impact from multiple accident scenarios. H3 has a lower death probability caused by toxic gas because it is located far away from T1 and it is also not close to any of the storage tanks. Contrarily, fire can escalate from tanks nearby T1 to the tanks close to H5 although there is a long distance between T1 and H5. As a result, H5 may die due to fire and
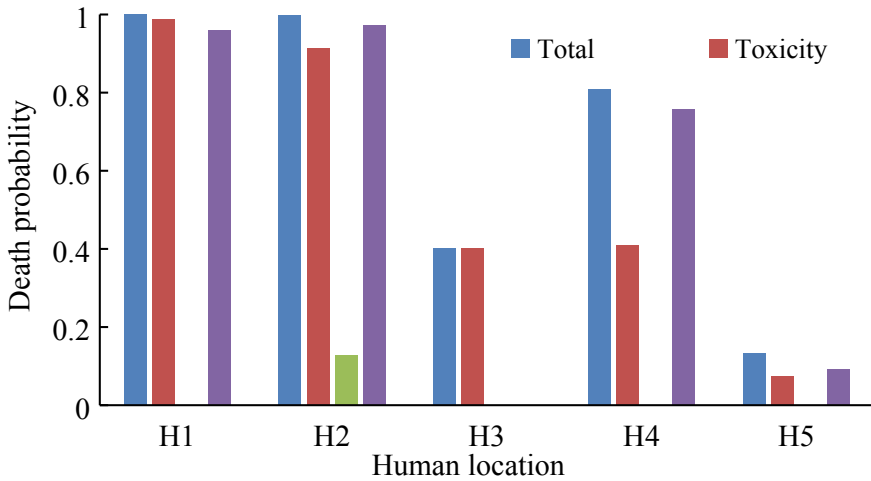
**Fig. 4.6**  Death probabilities caused by different accident scenarios at H1–H5 (Chen et al. [1])

toxic gas. According to these results, different personal protective equipment (PPE) can be assigned to people in different locations or at different times. For instance, people at H3 only need to take a gas mask while protective clothing against potential heat is also needed for people at H1, H2, H4, and H5.

## 4.5   Conclusions

This chapter develops a dynamic graph Monte Carlo (DGMC) model to model the evolution of coupled hazardous scenarios and assess the vulnerability of humans and facilities. The DGMC model can effectively model simultaneous or sequential multiple hazardous scenarios caused by coupled domino effects. Suppose only one type of scenario is considered in coupled domino effects. In that case, the vulnerability of installations and humans may be primarily underestimated, resulting in the unreasonable allocation of personal protection equipment (PPE) and safety barriers. Since humans in different positions may suffer from different hazardous scenarios, different protection strategies should be implemented for people in different positions; According to the application of the developed model [1], VCEs may result in the damage of multiple hazardous installations and the safety distances based on fire hazards may not be sufficient for VCEs; Furthermore, humans close to the release source are prone to multiple hazardous scenarios while acute toxicity and VCEs are the main causes for the deaths outside the release areas.

# References

1. Chen C, Reniers G, Khakzad N (2021) A dynamic multi-agent approach for modeling the evolution of multi-hazard accident scenarios in chemical plants. Reliab Eng Syst Saf 207
2. Chen C (2021) A dynamic and integrated approach for modeling and managing domino-effects. Delft University of Technology
3. Chen C, Reniers G, Khakzad N (2019) Integrating safety and security resources to protect chemical industrial parks from man-made domino effects: a dynamic graph approach. Reliab Eng Syst Saf 191
4. Wang B, Li D, Wu C (2020) Characteristics of hazardous chemical accidents during hot season in China from 1989 to 2019: a statistical investigation. Saf Sci 129
5. Yang Y, Chen G, Reniers G (2019) Vulnerability assessment of atmospheric storage tanks to floods based on logistic regression. Reliab Eng Syst Saf 106721
6. Wang B, Wu C, Reniers G, Huang L, Kang L, Zhang L (2018) The future of hazardous chemical safety in China: opportunities, problems, challenges and tasks. Sci Total Environ 643:1–11
7. Vilchez JA, Sevilla S, Montiel H, Casal J (1995) Historical analysis of accidents in chemical plants and in the transportation of hazardous materials. J Loss Prev Process Ind 8(2):87–96
8. Mishra KB, Wehrstedt K-D, Krebs H (2013) Lessons learned from recent fuel storage fires. Fuel Process Technol 107:166–172
9. Mishra KB, Wehrstedt K-D, Krebs H (2014) Amuay refinery disaster: the aftermaths and challenges ahead. Fuel Process Technol 119:198–203
10. Maremonti M, Russo G, Salzano E, Tufano V (1999) Post-accident analysis of vapour cloud explosions in fuel storage areas. Process Saf Environ Prot 77(6):360–365
11. Taveau J (2012) The Buncefield explosion: were the resulting overpressures really unforeseeable? Process Saf Prog 31(1):55–71
12. Sharma RK, Gurjar BR, Wate SR, Ghuge SP, Agrawal R (2013) Assessment of an accidental vapour cloud explosion: lessons from the Indian Oil Corporation Ltd. accident at Jaipur, India. J Loss Prev Process Ind 26(1):82–90
13. Dasgotra A, Varun Teja GVV, Sharma A, Mishra KB (2018) CFD modeling of large-scale flammable cloud dispersion using FLACS. J Loss Prev Process Ind 56:531–536
14. Mishra KB (2018) The influence of volume blockage ratio on IOCL Jaipur explosion. J Loss Prev Process Ind 54:196–205
15. Gant SE, Atkinson GT (2011) Dispersion of the vapour cloud in the Buncefield Incident. Process Saf Environ Prot 89(6):391–403
16. Salzano E, Cozzani V (2003) The use of probit functions in the quantitative risk assessment of domino accidents caused by overpressure. Saf Reliab 1 and 2. A Balkema Publishers, Leiden
17. Cozzani V, Salzano E (2004) The quantitative assessment of domino effects caused by overpressure: Part I. Probit models. J Hazard Mater 107(3):67–80
18. Cozzani V, Salzano E (2004) The quantitative assessment of domino effect caused by overpressure: Part II. Case studies. J Hazard Mater 107(3):81–94
19. Zhang M, Jiang J (2008) An improved probit method for assessment of domino effect to chemical process equipment caused by overpressure. J Hazard Mater 158(2–3):280–286
20. Mukhim ED, Abbasi T, Tauseef SM, Abbasi SA (2017) Domino effect in chemical process industries triggered by overpressure—formulation of equipment-specific probits. Process Saf Environ Prot 106:263–273
21. Zhou J, Reniers G (2017) Petri-net based cascading effect analysis of vapor cloud explosions. J Loss Prev Process Ind 48:118–125
22. Yang Y, Chen G, Chen P (2018) The probability prediction method of domino effect triggered by lightning in chemical tank farm. Process Saf Environ Prot 116:106–114
23. Khakzad N, Landucci G, Reniers G (2017) Application of graph theory to cost-effective fire protection of chemical plants during domino effects. Risk Anal 37(9):1652–1667
24. Khakzad N, Reniers G, Abbassi R, Khan F (2016) Vulnerability analysis of process plants subject to domino effects. Reliab Eng Syst Saf 154:127–136

25. Landucci G, Gubinelli G, Antonioni G, Cozzani V (2009) The assessment of the damage probability of storage tanks in domino events triggered by fire. Accid Anal Prev 41(6):1206–1215
26. Khakzad N (2015) Application of dynamic Bayesian network to risk analysis of domino effects in chemical infrastructures. Reliab Eng Syst Saf 138:263–272
27. Chen C, Reniers G, Zhang L (2018) An innovative methodology for quickly modeling the spatial-temporal evolution of domino accidents triggered by fire. J Loss Prev Process Ind 54:312–324
28. Kamil MZ, Taleb-Berrouane M, Khan F, Ahmed S (2019) Dynamic domino effect risk assessment using Petri-nets. Process Saf Environ Prot 124:308–316
29. Zeng T, Chen G, Yang Y, Chen P, Reniers G (2019) Developing an advanced dynamic risk analysis method for fire-related domino effects. Process Saf Environ Prot
30. Zhang L, Landucci G, Reniers G, Khakzad N, Zhou J (2018) DAMS: a model to assess domino effects by using agent-based modeling and simulation. Risk Anal 38(8):1585–1600
31. Abdolhamidzadeh B, Abbasi T, Rashtchian D, Abbasi SA (2010) A new method for assessing domino effect in chemical process industry. J Hazard Mater 182(1–3):416–426
32. Rad A, Abdolhamidzadeh B, Abbasi T, Rashtchian D (2014) FREEDOM II: an improved methodology to assess domino effect frequency using simulation techniques. Process Saf Environ Prot 92(6):714–722
33. Bonabeau E (2002) Agent-based modeling: methods and techniques for simulating human systems. Proc Natl Acad Sci 99(suppl 3):7280–7287
34. Rai S, Hu X (2018) Hybrid agent-based and graph-based modeling for building occupancy simulation. In: Proceedings of the 4th ACM international conference of computing for engineering and sciences, pp 1–12
35. Stroeve SH, Blom HA, Bakker GB (2013) Contrasting safety assessments of a runway incursion scenario: event sequence analysis versus multi-agent dynamic risk modelling. Reliab Eng Syst Saf 109:133–149
36. Harary F (1969) Graph theory. Addison-Wesley, Reading, MA
37. Jafari S, Ajorlou A, Aghdam AG (2011) Leader localization in multi-agent systems subject to failure: a graph-theoretic approach. Automatica 47(8):1744–1750
38. Ding L, Ji J, Khan F (2020) Combining uncertainty reasoning and deterministic modeling for risk analysis of fire-induced domino effects. Saf Sci 129
39. Jiang D, Wu B, Cheng Z, Xue J, van Gelder PHAJM (2020) Towards a probabilistic model for estimation of grounding accidents in fluctuating backwater zone of the Three Gorges Reservoir. Reliab Eng Syst Saf
40. Khakzad N, Reniers G (2015) Using graph theory to analyze the vulnerability of process plants in the context of cascading effects. Reliab Eng Syst Saf 143:63–73
41. Rubinstein RY, Kroese DP (2016) Simulation and the Monte Carlo method, vol 10. Wiley
42. Joy DC (1995) Monte Carlo modeling for electron microscopy and microanalysis, vol 9. Oxford University Press
43. Kuczera G, Parent E (1998) Monte Carlo assessment of parameter uncertainty in conceptual catchment models: the Metropolis algorithm. J Hydrol 211(1–4):69–85
44. Van Den Bosh C, Merx W, Jansen C, De Weger D, Reuzel P, Leeuwen D, Blom-Bruggerman J (1989) Methods for the calculation of possible damage (Green Book). Committee for the Prevention of Disasters, The Hague (NL)
45. Uijt de Haag, Ale (1999) Guidelines for quantitative risk assessment. Committee for the Prevention of Disasters, The Hague (NL)
46. Atkinson G, Coldrick S (2012) Vapour cloud formation: experiments and modelling. Health and Safety Laboratory, Debyshire
47. Chen C, Khakzad N, Reniers G (2020) Dynamic vulnerability assessment of process plants with respect to vapor cloud explosions. Reliab Eng Syst Saf 200
48. Brazdil JF (2000) Acrylonitrile. Ullmann's encyclopedia of industrial chemistry